BIOCHEMISTRY
including biophysical chemistry & molecular biology

Article

pubs.acs.org/biochemistry

The Kinase Activity of the *Helicobacter pylori* Asp-tRNA^{Asn}/Glu-tRNA^{Gln} Amidotransferase Is Sensitive to Distal Mutations in Its Putative Ammonia Tunnel

Liangjun Zhao, Sajeewa W. Dewage, Michael J. Bell,[†] Keng-Ming Chang,[‡] Shirin Fatma, Nilesh Joshi, Gayathri Silva, G. Andrés Cisneros,* and Tamara L. Hendrickson*

Department of Chemistry, Wayne State University, 5101 Cass Avenue, Detroit, Michigan 48202, United States

Supporting Information

ABSTRACT: The *Helicobacter pylori* (*Hp*) Asp-tRNA^{Asn}/Glu-tRNA^{Gln} amidotransferase (AdT) plays important roles in indirect aminoacylation and translational fidelity. AdT has two active sites, in two separate subunits. Kinetic studies have suggested that interdomain communication occurs between these subunits; however, this mechanism is not well understood. To explore domain−domain communication in AdT, we adapted an assay and optimized it to kinetically characterize the kinase activity of *Hp* AdT. This assay was applied to the analysis of a series of point mutations at conserved positions throughout the putative AdT ammonia tunnel that connects the two active sites. Several mutations that caused significant decreases in AdT's kinase activity (reduced by 55−75%) were identified. Mutations at Thr149 (37 Å distal to the GatB kinase active site) and Lys89 (located at the interface of GatA and GatB) were detrimental to AdT's kinase activity, suggesting that these mutations have disrupted interdomain communication between the two active sites. Models of wild-type AdT, a valine mutation at Thr149, and an arginine mutation at Lys89 were subjected to molecular dynamics simulations. A comparison of wild-type, T149V, and K89R AdT simulation results unmasks 59 common residues that are likely involved in connecting the two active sites.

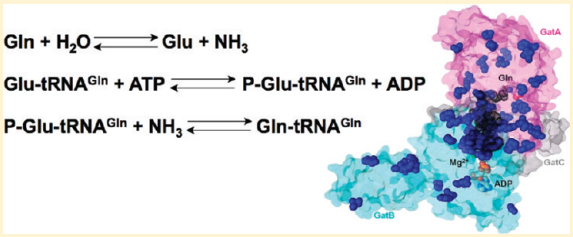

The discovery of the first molecular tunnel, in tryptophan synthase, challenged the conventional mechanism of multiple-active site enzymes.[1] In contrast to ligand-induced conformational changes that bring multiple active sites into proximity of each other, some enzymes have evolved molecular tunnels for connecting isolated catalytic centers.[2−4] These tunnels can enhance the stability of reactive intermediates via sequestration and allow the delivery of intermediates to the next active site. Furthermore, tunnels can serve as a method of interdomain communication, in which the binding of the substrate or the generation of an intermediate at one active site triggers conformational changes at another, distal active site.[2−5]

Most glutamine-dependent amidotransferases (GATs) contain molecular tunnels. These enzymes play important roles in diverse biosynthetic pathways as they deliver ammonia from the side chain of glutamine to various electrophilic acceptors during the biosynthesis of cofactors,[6−8] amino acids,[9−11] amino sugars,[12] purines,[13] and pyrimidines,[14] among others. The tunnels serve to sequester and deliver ammonia (generated via glutamine hydrolysis in one active site) to the downstream active site. Crystal structures are available for many of these enzymes and reveal that the molecular tunnels are typically hydrophobic or only partially occupied by water;[1,15−20] they range in length from 6 Å (e.g., glucosamine 6-phosphate synthase[19]) to 45 Å (e.g., carbamoyl phosphate synthetase[20]).

Helicobacter pylori Asp-tRNA^{Asn}/Glu-tRNA^{Gln} amidotransferase (AdT) is a heterotrimeric GAT made up of the GatC, GatA, and GatB subunits.[21] Like many bacteria, *H. pylori* is missing both glutaminyl- and asparaginyl-tRNA synthetase (GlnRS and AsnRS, respectively).[22,23] In these species, AdT is essential for protein translation and fidelity because it converts the misacylated tRNAs Glu-tRNA^{Gln} and Asp-tRNA^{Asn} into Gln-tRNA^{Gln} and Asn-tRNA^{Asn}, respectively.[21,24,25] AdT catalyzes three distinct reactions. The GatA subunit contains a classic amidase signature sequence and catalyzes the hydrolysis of glutamine into glutamate and ammonia (reaction 1).[21] The GatB active site catalyzes phosphorylation and transamidation of both Glu-tRNA^{Gln} and Asp-tRNA^{Asn} (reactions 2 and 3, respectively, shown for Glu-tRNA^{Gln} only).[26] GatC is apparently not involved in catalysis.

$$\text{(GatA):}\quad \text{Gln} \leftrightarrows \text{Glu} + \text{NH}_3 \tag{1}$$

$$\text{(GatB):}\quad \text{Glu-tRNA}^{\text{Gln}} + \text{ATP} \leftrightarrows \text{phospho-Glu-tRNA}^{\text{Gln}} + \text{ADP} \tag{2}$$

$$\text{(GatB):}\quad \text{phospho-Glu-tRNA}^{\text{Gln}} + \text{NH}_3 \leftrightarrows \text{Gln-tRNA}^{\text{Gln}} + \text{P}_\text{i} \tag{3}$$

Received: July 25, 2011
Revised: December 12, 2011
Published: December 15, 2011

ACS Publications © 2011 American Chemical Society

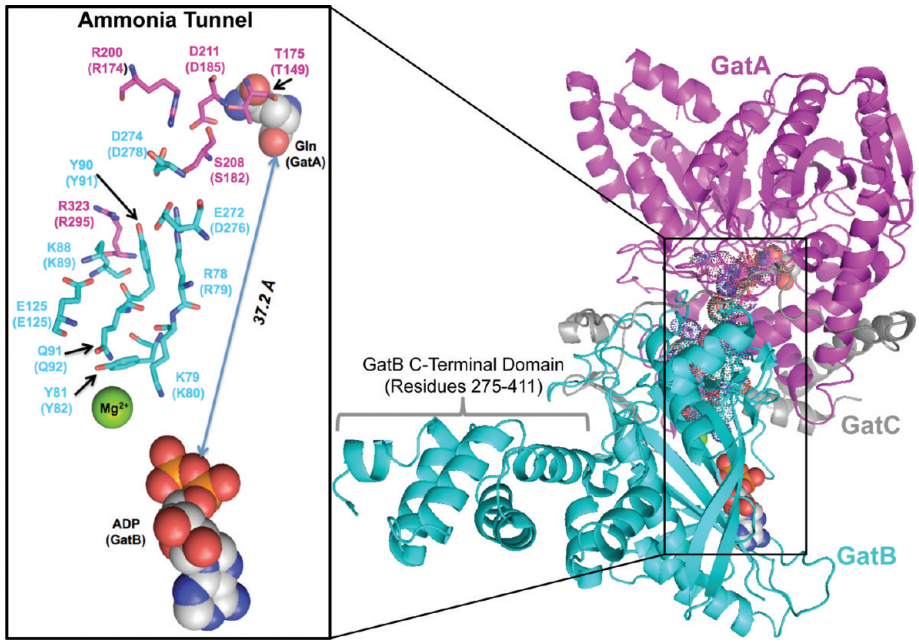

Figure 1. Structure of the *S. aureus* AdT and its putative ammonia tunnel. This image was built from the *S. aureus Mu50* AdT crystal structure using Pymol and PDB entries 2F2A and 2G5I. GatA is colored magenta, GatB cyan, and GatC gray. Conserved residues along the proposed tunnel are highlighted as sticks and dots.[43] The glutamine in the GatA active site (from PDB entry 2F2A) and the ADP in the GatB active site (from PDB entry 2G5I) are shown as space-filled molecules. The GatB C-terminal flexible domain (residues 275−411) is indicated; see the text for details. The inset shows a close-up of the conserved residues lining the ammonia tunnel. The residues are numbered according to *S. aureus Mu50* AdT, with parenthetical notations indicating the corresponding positions in *H. pylori* AdT.

The crystal structure of *Staphylococcus aureus* AdT revealed that the GatA and GatB active sites are separated by 37 Å, and a putative ammonia tunnel that connects the two catalytic centers was identified (Figure 1).[26] This tunnel is unique, compared to other known ammonia tunnels,[2] because it is highly populated with ordered water molecules and lined with conserved polar and ionic amino acids.[26] Tanaka and colleagues proposed that ammonia delivery could occur through a series of protonation and deprotonation events.[26] To the best of our knowledge, such a mechanism would be unprecedented among enzymes that utilize ammonia tunnels.

In many respects, AdT is well-characterized for its role in indirect tRNA aminoacylation, translational fidelity, catalysis, specificity for both Asp-tRNA^{Asn} and Glu-tRNA^{Gln}, and the formation of a transamidosome complex with a nondiscriminating aspartyl-tRNA synthetase (ND-AspRS).[25,27,28] In contrast, little is known about whether the GatA and GatB subunits communicate with each other, except that the addition of ATP and Glu-tRNA^{Gln} stimulates the glutaminase activity of GatA.[25,29]

AdT's kinase and glutaminase reactions must both occur before transamidation. We hypothesized that GatB's kinase activity might serve as a probe for examination of the domain−domain connectivity between the GatA and GatB active sites. We optimized and applied a UV-based colorimetric method[30,31] to the quantification of the kinase activity of AdT. This assay was used to kinetically characterize a series of mutations at conserved positions throughout the putative AdT tunnel. Effects ranged from negligible to an approximately 75% reduction in kinase activity. Mutations at T149 and K89 attracted our attention because even conservative mutations at these positions caused substantial decreases in kinase activity in GatB. This effect was essentially the same whether rates were measured in the presence or absence of glutamine. Additionally, T149 is located at the entrance of the ammonia tunnel in GatA distal to the GatB kinase active site, and K89 lies at the interface of GatA and GatB. Our kinetic analyses of these mutations suggest that they participate in directing communication between the glutaminase and kinase active sites of AdT.

To investigate this domain−domain communication, we conducted molecular dynamics (MD) simulations on wild-type (WT), T149V, and K89R AdT, all with and without glutamine bound to the glutaminase active site. Root-mean-square deviation (RMSD) and residue-wise correlation analyses indicate a significant difference in structural mobility for certain regions in the mutant structures compared to the wild-type enzyme. This effect is more pronounced when Gln is bound in the glutaminase active site of T149V AdT in contrast to the observed steady-state kinetic measurements. Analyses of the simulation results point to 59 AdT residues that show an elevated level of mobility in both T149V and K89R AdT variants. These residues cluster mainly along the tunnel or close to the tRNA binding site. Taken together with our kinetic analyses, these results strongly suggest a pathway for domain−domain communication in AdT.

MATERIALS AND METHODS

Materials. Oligonucleotides were purchased from Invitrogen and used without further purification. Pfu polymerase was purchased from Stratagene. Taq polymerase was from New England Biolabs. All buffers were filtered through a 0.22 μm filter prior to use. When appropriate, solutions were autoclaved. Unless otherwise stated, reagents were used without further purification.

Cloning of *Hp* AdT. The *H. pylori gatCAB* operon was originally amplified from *H. pylori* strain 26695. The genes encoding the three subunits of AdT were subcloned into two compatible plasmids (S. Skouloubris and P. Chuawong,

unpublished results). Plasmid pPTC032 is derived from pCDF-1b (Novagen) and encodes GatC and GatA in a single operon with an N-terminal six-histidine (His_6) tag appended onto GatC. Plasmid pSS003 (derived from pET-28a) encodes GatB with an N-terminal six-histidine tag (pPTC032).

Site-Directed Mutagenesis. Individual point mutations were introduced into either the *gatA* or *gatB* gene (encoded by plasmid pPTC032 or pSS003, respectively) by QuikChange mutagenesis according to the directions provided by Stratagene. Oligonucleotide sequences and plasmids are listed in Table S1 of the Supporting Information. All gene constructs were verified by DNA sequencing of the entire gene prior to use.

Overexpression and Purification of *Hp* AdT. For wild-type AdT, *Escherichia coli* strain BL21(DE3) calcium chloride competent cells were transformed with both pPTC032 and pSS003. For expression of each mutant AdT, BL21(DE3) was first transformed with the plasmid encoding the wild-type subunit(s) and then individually transformed with each mutated plasmid. For example, to produce the T149A AdT mutant, cells were transformed with pSS003, encoding wild-type His_6-GatB, and then with plasmid pSF005, encoding His_6-GatC and T149A GatA in an operon. In all cases, colonies containing both plasmids were selected on agar plates supplemented with kanamycin (50 μg/mL) and streptomycin (50 μg/mL) and incubated at 37 °C overnight. A 5 mL Luria Broth (LB) culture, containing the same two antibiotics, was inoculated with a single colony. The overnight culture was scaled up to 500 mL in the same medium. When the absorbance at 600 nm was between 0.4 and 0.6, IPTG was added to a final concentration of 1 mM to induce overexpression. Cells were harvested by centrifugation at 5000 rpm for 5 min at 4 °C after a 4 h induction, and AdT or its mutants were purified by HisPur Cobalt resin (Pierce) by following the manufacturer's instructions. With the exception of R174A AdT, all mutations were readily purified to homogeneity (see Figure S1 of the Supporting Information). Protein concentrations were determined by UV–vis spectroscopy with the extinction coefficients for each protein determined using the ExPASy Proteomics server (http://ca.expasy.org/tools/protparam.html).[32]

In Vivo Transcription of *H. pylori* tRNA^{Gln} and tRNA Purification. *H. pylori* tRNA^{Gln} was transcribed in vivo in *E. coli* strain MV1184, and the tRNA was purified and quantified as previously described.[33]

Preparation of Glu-tRNA^{Gln}. *H. pylori* tRNA^{Gln} was aminoacylated with glutamate using *H. pylori* GluRS2[33] as previously described.[34] The resultant product was extracted with a phenol/chloroform mixture (1/1); excess ATP and ADP were removed as previously described.[35] The Glu-tRNA^{Gln} yield was quantified by running a parallel reaction mixture that contained ^{3}H-labeled glutamic acid.

AdT Kinase Assay. The kinase activity of AdT was monitored via adaptation of a coupled enzyme assay (Figure 2A).[30,31] Unless otherwise stated, assays were performed at room temperature in buffer containing 20 mM HEPES-KOH (pH 7.5), 5 mM $MgCl_2$, 0.1 mM DTT, 2 mM phosphoenolpyruvate (PEP), 2 mM ATP, 20 units/mL pyruvate kinase (PK), 20 units/mL L-lactate dehydrogenase (LDH), and NADH to give an absorbance of 0.3–0.4 at 340 nm (between 50 and 70 μM, based on standards at known concentrations). For initial rate determinations, saturating concentrations of Glu-tRNA^{Gln} (10 μM) were used so that the observed initial rates would approximate k_{cat} for each residue. This approach allowed us to focus our analysis on catalytic defects that were conveyed across distances through the enzyme. The possibility that K_M is altered for one or more mutations cannot be ruled out but was not expected to impact data analysis; these values may be determined at a later date. For Michaelis–Menten analyses, the concentration of Glu-tRNA^{Gln} was varied from 0 to 8 μM and the concentration of AdT was held constant at 300 nM. All other assays were initiated with 200 nM AdT enzyme. Reaction progress was monitored on a Beckman DU 800 spectrometer at 340 nm. Full Michaelis–Menten values were determined only for wild-type AdT.

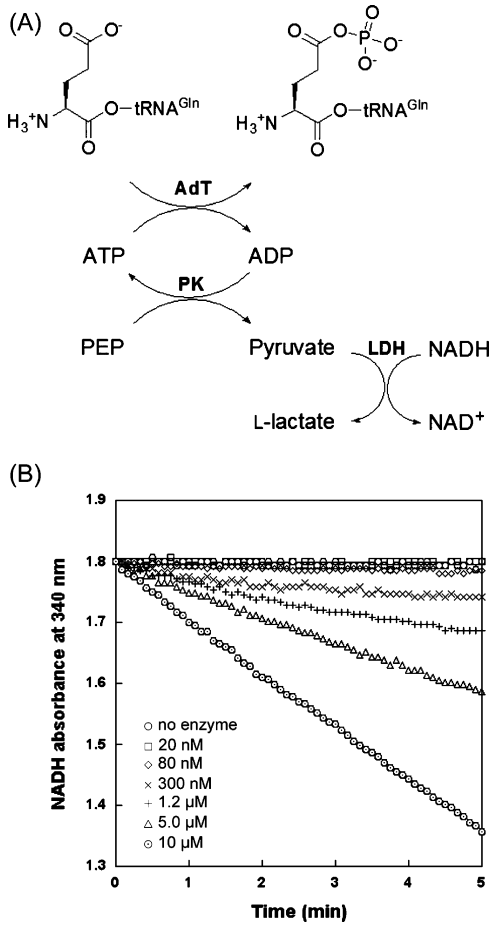

Figure 2. Coupled enzyme assay for measuring AdT's phosphorylation activity with Glu-tRNA^{Gln}. (A) Assay schematic. The hydrolysis of ATP is coupled to the oxidation of NADH; the resultant decrease in NADH concentration is monitored by UV at 340 nm. (B) The assay is responsive over a wide range of AdT concentrations: (○) no enzyme, (□) 20 nM, (◇) 80 nM, (×) 300 nM, (+) 1.2 μM, (△) 5.0 μM, and (⊙) 10 μM.

As part of the optimization of this assay, wild-type AdT concentrations were varied from 0 to 10 μM to confirm that the coupling enzyme conditions were reporting kinase activity (rather than the activities of PK or LDH). Additionally, the NADH concentration was optimized (reduced from 200 to <70 μM) to produce the largest observable change in absorbance without impacting the actual rate of phosphorylation; this optimization led to more accurate and reproducible results.

Molecular Dynamics Simulations of AdT and the Two Mutants. All molecular dynamics (MD) simulations were performed with the PMEMD program in the AMBER11 software suite with the amber99SB force field.[36] The SHAKE

algorithm[37] was applied on all bonds between heavy atoms and hydrogens. All the simulations were conducted under periodic boundary conditions, and the smooth particle mesh Ewald method was used to account for long-range interactions.[38,39]

The crystal structure of AdT from *S. aureus* was taken from PDB entry 2F2A.[26] This crystal structure was chosen because there are no reported crystal structures for *H. pylori* AdT and it is highly homologous to that of *S. aureus* AdT. The crystal structure was checked and protonated with MolProbity.[40] Protein termini for all subunits and the glutamine substrate bound to GatA (when present) were capped using acetyl (ACE) and *N*-methyl acetamide (NME) groups.

The simulated systems included wild-type, T149V, and K89R AdT in the presence or absence of glutamine. On the basis of the protein sequence alignment of *H. pylori* and *S. aureus* AdT (see Figure S4 of the Supporting Information), residue T175 in *S. aureus*, homologous to T149 in *H. pylori*, was replaced with valine in the mutant structures and residue K88 in *S. aureus*, homologous to K89 in *H. pylori*, was replaced with arginine in the mutant structures. All structures were created using the UCSF Chimera software suite.[41]

The protonated structures were minimized using the sander program in AMBER with 50 steps of steepest descent and 450 steps of conjugate gradient with constraints on the protein (a force constant of 500 kcal mol^{-1} $Å^{-2}$ on the protein). The minimized structures were solvated using the TIP3P water model inside 125 Å × 96 Å × 142 Å rectangular boxes. Charges were neutralized in all four structures by adding Na^+ ions using the xleap program in AMBER.

The added water molecules were minimized again using the PMEMD program in AMBER with 50 steps of steepest descent and 450 steps of conjugate gradient minimization. During this minimization, the protein and substrates were restrained with a force constant of 500 kcal mol^{-1} $Å^{-2}$.

Following minimization, the density of all the systems was increased to 1 g/cm^3 by NPT simulations restraining all protein and substrate atoms with a force constant of 500 kcal mol^{-1} $Å^{-2}$. The pressure was kept constant by anisotropic pressure.[36] Subsequently, the systems were gradually heated to 300 K in 10 steps (10 ps each) at a constant volume with constraints on the protein (500 kcal mol^{-1} $Å^{-2}$ force constant on the protein). For the wild-type without glutamine bound to the GatA active site, the warm-up was performed in 10 steps of 20 ps each. Once the systems achieved the target temperature, the constraints were gradually removed over 80 ps until no constraints were left. The temperature was kept constant using a Berendsen thermostat.[42] Subsequently, simulations were conducted for an additional 20 ns for each system with snapshots taken every 1 ps.

RESULTS

Production of *H. pylori* AdT and Its Mutants. Initially, the *gatCAB* genes were assembled into a single operon in the pET-28a vector; a plasmid (pSS003) encoding only His_6-GatB (also in pET-28a) was also constructed (S. Skouloubris, unpublished results). To facilitate purification, and building from a previous report,[28] we transplanted the *gatCA* operon into the pCDF-1b vector (compatible with pET-28a) with concomitant addition of an N-terminal His_6 tag onto GatC (His_6-GatC, pPTC032). The two resultant plasmids were cotransformed into *E. coli*, and wild-type AdT was readily purified to homogeneity, essentially as previously reported (see Figure S1 of the Supporting Information).[28] Following purification, the ratio of GatA to GatB was examined to ensure that AdT concentrations were not inaccurate because of a dramatic excess of one subunit over the other.

Each mutant was purified using the same approach optimized for wild-type AdT (see Figure S1 of the Supporting Information). For GatA mutations, plasmid pSS003 was separately transformed with each mutant variant of pPTC032. For GatB mutations, plasmid pPTC032 was separately cotransformed with each mutant variant of pSS003 (see Table S1 of the Supporting Information for the list of mutant plasmids).

Development of a Coupled Enzyme Assay for AdT-Catalyzed Phosphorylation of Glu-tRNA^{Gln}. Conversion of ATP into ADP can be observed indirectly via a coupled, spectroscopic enzyme assay that monitors the oxidation of NADH to NAD^+ (Figure 2A).[31] In this assay, AdT-catalyzed phosphorylation of Glu-tRNA^{Gln} causes concomitant production of ADP. ATP is regenerated in the presence of excess phosphoenolpyruvate (PEP) and pyruvate kinase (PK), to produce pyruvate. Lactate dehydrogenase (LDH) reduces the resultant pyruvate to L-lactate, via conversion of NADH to NAD^+. This reaction can be monitored spectrophotometrically because NADH has an absorbance maximum at 340 nm and NAD^+ does not absorb UV light at this wavelength.

Coupled enzyme assays carry the risk that one is inadvertently quantifying the activity of the downstream enzyme(s) (LDH and/or PK in this case), rather than the enzyme of interest (AdT). To rule out this concern, we conducted several control experiments before progressing with quantitative assays of AdT and its mutants. The previously reported buffer conditions were adapted to those for AdT.[25] Different AdT enzyme concentrations were also examined (Figure 2B). As the concentration of AdT was increased (ranging from 20 nM to 10 μM), the rate of ATP hydrolysis also increased, confirming that the assay was directly reporting on AdT activity. Previously reported UV-based assays typically used NADH concentrations of 200 μM;[30] with AdT, this concentration led to an untenable signal-to-noise ratio (S/N) (see Figure S2A of the Supporting Information). To address this issue, we decreased the concentration of NADH to 50−70 μM. This reduction led to a much more acceptable S/N while producing the same rate of ATP hydrolysis [again, indicating that AdT activity, and not PK or LDH, is being reported (see Figure S2B of the Supporting Information)]. An NADH calibration curve (Figure S3 of the Supporting Information) allowed us to accurately correlate UV absorbance with concentration.

Michaelis−Menten Kinetics. The K_M of ATP is approximately 200 μM, when measuring the net reaction of *H. pylori* AdT (transamidation).[43] Thus, the concentration of ATP was set at 2 mM for all assays. Kinetic parameters were determined for Glu-tRNA^{Gln} as a substrate for AdT's kinase activity (Figure 3). The K_M for this misacylated tRNA is 1.6 ± 0.5 μM and is consistent with values previously reported (1.18 μM, determined by measuring AdT's transamidase activity[43]). The calculated k_{cat} is 0.12 ± 0.01 s^{-1}, leading to a specificity constant (k_{cat}/K_M) of 7.5 × 10^4 s^{-1} M^{-1} for the phosphorylation of Glu-tRNA^{Gln} in the absence of glutamine.

Design and Characterization of Mutations in the Putative AdT Tunnel. It has been proposed that ammonia is transferred from GatA to GatB through a protonation−deprotonation relay mechanism; this hypothesis is based on the observation that the putative ammonia tunnel contains

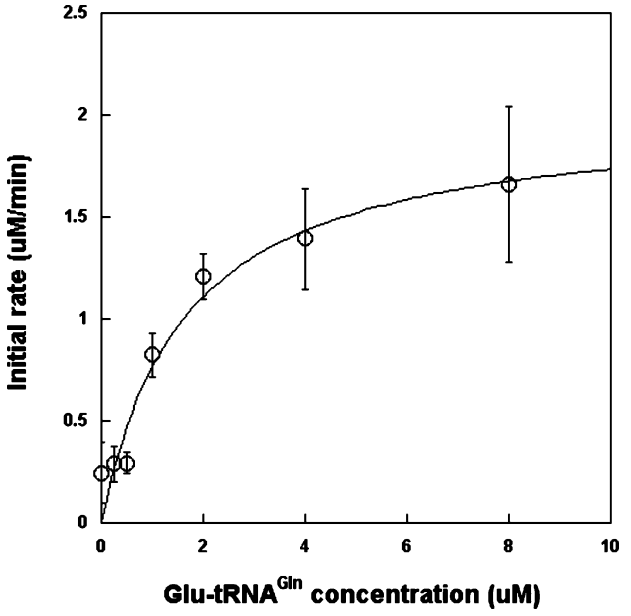

Figure 3. Michaelis–Menten analysis of Glu-tRNA^{Gln} as a substrate for AdT-catalyzed phosphorylation. Each reaction was initiated with 300 nM AdT. Data was fit directly to the Michaelis–Menten equation using Kaleidagraph version 4.0 (Synergy Software). Error bars represent the standard deviation and are from duplicate measurements. Standard deviations reported in the text are from the results of the curve fit analysis.

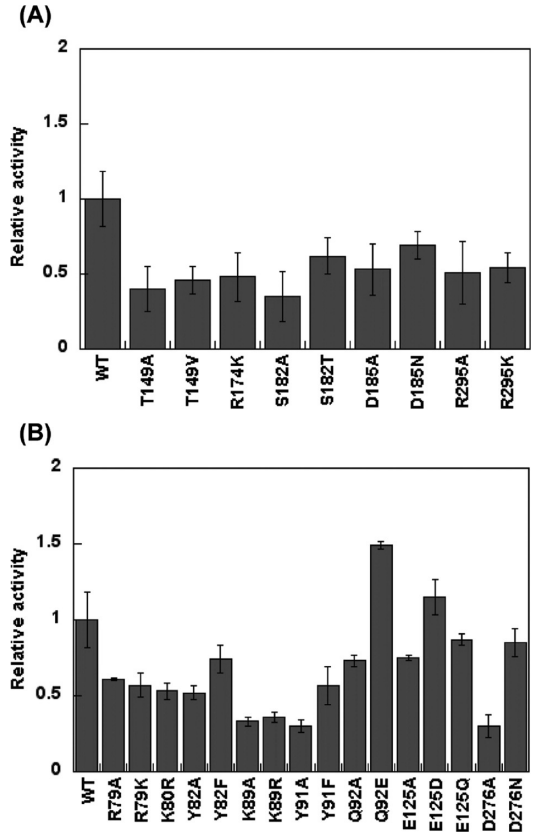

Figure 4. Steady-state initial rates of Glu-tRNA^{Gln} phosphorylation using wild-type *H. pylori* AdT and variants containing single point mutations along the ammonia tunnel. Initial rates, relative to that of wild-type AdT, are shown. See Table S2 of the Supporting Information for the raw initial rate data. The error bars represent the standard deviation from triplicate assays: (A) analysis of mutations in GatA and (B) analysis of mutations in GatB.

many hydrophilic and ionic residues and ordered water molecules.[26] The *H. pylori* and *S. aureus* AdT protein sequences were aligned (see Figure S4 of the Supporting Information). A protein sequence alignment between the *H. pylori* and *S. aureus* AdT subunits showed that the two GatA subunits are 45% identical and 75% similar and the two GatB subunits are 53% identical and 89% similar. A more detailed alignment identified 13 highly conserved residues along the putative ammonia tunnel (Table 1 and Figure 1).[26] Most of these amino acids were separately mutated to alanine and to one or more conservative amino acids to determine which, if any, of these positions is important for phosphorylation of Glu-tRNA^{Gln}.

Table 1. AdT Ammonia Tunnel Conserved Residues

S. aureus	*H. pylori*	*H. pylori* mutations
	GatA Mutagenesis	
T175	T149	T149A, -V, -S[a]
R200	R174	R174A,[b] -K
S208	S182	S182A, -T
D211	D185	D185A, -N
R323	R295	R295A, -K
	GatB Mutagenesis	
R78	R79	R79A, -K
K79	K80	K80A,[a] -R
Y81	Y82	Y82A, -F
K88	K89	K89A, -R
Y90	Y91	Y91A, -F
Q91	Q92	Q92A, -E
E125	E125	E125A, -D, -Q
E272[c]	D276	D276A, -N
D274	D278	*d*

[a]Site-directed mutagenesis was not successful. [b]The mutant could not be purified to homogeneity. [c]The residue is not rigorously conserved but is typically glutamic or aspartic acid. [d]Not analyzed.

Each mutant enzyme was purified to homogeneity, with the exception of R174A, which could not be purified sufficiently for further analysis because of poor expression levels (see Figure S1 of the Supporting Information). Initial rates of phosphorylation of Glu-tRNA^{Gln} were determined for each mutant enzyme using the coupled assay described above. Relative activities with respect to wild-type AdT were calculated and are shown in panels A and B of Figure 4. No single mutation was sufficient to completely abolish phosphorylation activity, including mutations at K80 and Y82 (*H. pylori* numbering), which are located near the ATP binding site. These results show that the ATP binding site is remarkably tolerant of mutations at conserved residues. However, several point mutations did cause dramatic reductions in activity (Figure 4), with some leading to decreases in initial rates of as much as 75%. Not surprisingly, in general, conservative mutations were less disruptive than the alanine screen. For example, the activity of Q92A is diminished by approximately 25% with respect to that of wild-type AdT; in contrast, the Q92E mutant is actually 50% more active than wild-type AdT, at least with respect to phosphorylation (Figure 4B). This increase might be due to simultaneous ATP hydrolysis caused by the mutation in parallel to the phosphorylation of Glu-tRNA^{Gln}, because Q92 is located near the ATP binding site.

dx.doi.org/10.1021/bi201143x | *Biochemistry* 2012, 51, 273–285

Discussions in the literature have suggested that E125 may[43] or may not[44] act as a gate, blocking AdT's ammonia tunnel to prohibit inadvertent ammonia release (e.g., in the absence of bound Glu-tRNA^{Gln}). Mutations at position E125 in GatB had little to no effect on AdT's phosphorylation activity (Figure 4B). These results demonstrate that the identity of E125 does not impact the steady-state rate of phosphorylation of Glu-tRNA^{Gln}; further experiments are necessary to determine if E125 plays a different kinetic role. When D276 (which lies near the midpoint of the putative ammonia tunnel) was mutated to alanine, the phosphorylation activity of the resulting enzyme was only 30% of that of wild-type AdT. In contrast, the D276N mutation maintained 85% of the wild-type enzyme's activity. S182A, in GatA, also showed a large reduction in phosphorylation activity (35% that of wild-type), but this activity was partially recovered in the S182T mutant (to 62% that of wild-type). Further analyses of these mutations are ongoing.

Mutagenesis at a few positions revealed a strong, deleterious response even upon the introduction of conservative mutations [e.g., T149 (GatA), R295 (GatA), K89 (GatB), and Y91 (GatB)]. Three of these residues (R295, K89, and Y91) are localized at the interface between GatA and GatB (Figure 1). Remarkably, T149 is adjacent to the glutaminase active site, at the top of the tunnel in GatA, substantially removed from the GatB active site. T149A AdT and T149V AdT demonstrated initial rates of phosphorylation that were 40 and 46% of that of wild-type AdT, respectively, while K89A and K89R AdT both caused ~65% decreases in the initial rates of phosphorylation. The kinase activity decrease caused by mutations at the distal T149 residue indicates the possibility of interdomain communication. The results with K89 mutations are also interesting because this residue is adjacent to E125, the putative gate (see below for further analyses of these mutations).

Effects of Glutamine on *H. pylori* AdT's Kinase Activity. All AdT mutations were originally screened in the absence of glutamine (Figure 4). The phosphorylation activities of representative mutations and wild-type AdT were reevaluated in the presence of 5 mM glutamine to determine if this GatA active site substrate positively or negatively impacts the activity of any of these mutant enzymes (Figure 5). Wild-type AdT and most mutants showed a slight, reproducible reduction in activity in the presence of glutamine. However, this reduction was only significant for the R295A, K89A, and Y91F mutations, all of which lie at the interface of the two subunits.

Molecular Dynamics Simulations of Wild-Type, T149V, and K89R AdT. T149 is located in the GatA active site, 37 Å from the site of ATP binding and Glu-tRNA^{Gln} phosphorylation in GatB. The fact that the kinase activity of AdT is sensitive to both valine and alanine substitutions of T149, despite the distance between this residue and the GatB active site, suggests that the hydroxyl group in the T149 side chain may play an essential role for proper domain−domain communication [attempts to produce a T149S mutation, to further evaluate this hypothesis, were unsuccessful (data not shown)].

Mutagenesis at residue K89, located in GatB near the interface between GatA and GatB, also resulted in a deleterious effect on kinase activity even upon introduction of a conservative mutation (K89R). One possible explanation is that the bulkier side chain of arginine (compared to lysine) might block the AdT ammonia tunnel, resulting in the observed decrease in enzymatic activity.

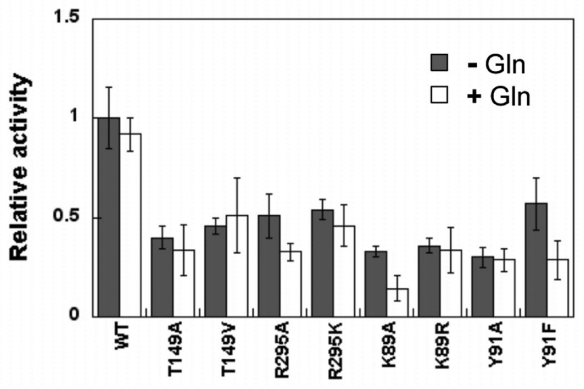

Figure 5. Effect of glutamine on the kinase activity of wild-type AdT and selected mutants (T149A, T149V, R295A, and R295K in GatA; K89A, K89R, Y91A, and Y91F in GatB). Initial rates relative to that of wild-type AdT were determined in the absence and presence of glutamine (5 mM). Error bars represent the standard deviation from triplicate assays. See Table S3 of the Supporting Information for the raw initial rate data.

To improve our understanding of the role of these mutations on AdT, wild-type, T149V, and K89R AdT models were subjected to molecular dynamics (MD) simulations. MD simulations were performed on six systems, and they were examined using the AMBER software suite: (1) wild-type AdT without glutamine bound to GatA, (2) wild-type AdT with bound glutamine, (3) T149V AdT without glutamine, (4) T149V AdT with bound glutamine, (5) K89R AdT without glutamine, and (6) K89R AdT with bound glutamine. Simulations were conducted as described in Materials and Methods.

Residue-wise correlation studies were conducted for each of the six simulated systems (Figure 6). The figure is colored to separately denote both positive (red) and negative (blue) correlations. A positive correlation result indicates that the movement of the two residues is concerted and they both move in the same direction (e.g., both side chains have rotated in a clockwise direction compared to the original crystal structure). A negative correlation result also indicates concerted movement; however, in this case, the two residues move in opposing directions (e.g., one side chain rotates clockwise and the other counterclockwise). In other words, correlation scores of 0.7 and −0.7 indicate the same extent of correlation, but in synergistic and opposing directions, respectively.

To more readily visualize the specific correlation changes throughout each mutant enzyme, correlation differences were calculated by subtracting the wild-type correlation values from those of each mutant (Figure 7). These correlation difference maps show that there are changes in correlation between the wild-type and mutant structures in all cases. These changes are most significant for the T149V mutant with glutamine bound to GatA, where strong anticorrelations between GatA and GatB are observed. The intensity of these correlation changes demonstrates that the identity of the T149 residue in GatA (in this case, the T149V mutation) is propagated throughout much of GatB, clearly demonstrating a physical connection between the two active sites. Although changes in correlation are observed in the T149V mutant without glutamine in the GatA active site, these changes are less dramatic. This observation is in contrast to the experimental results for the phosphorylation rates with Glu-tRNA^{Gln} where there were no

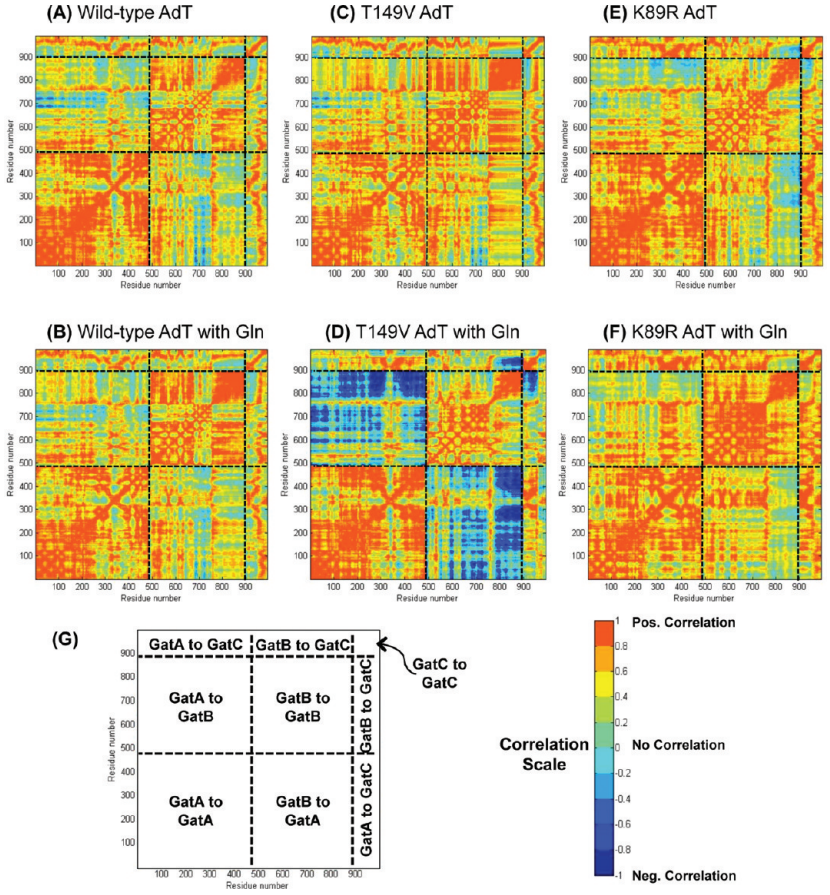

Figure 6. Residue-by-residue correlation analysis for all simulated structures: (A) wild-type AdT, (B) wild-type AdT with glutamine bound to GatA, (C) T149V AdT, (D) T149V AdT with glutamine, (E) K89R AdT, and (F) K89R AdT with glutamine. (G) Cartoon showing different regions of correlation; residues proceed from left to right (N-terminal to C-terminal, respectively) with GatA residues numbered 1−485, GatB residues numbered 486−897, and GatC residues numbered 898−991. All panels apply the same color-coded scale representing the correlation coefficient that stands for how one residue moves with respect to another. Correlation coefficients of 1 and −1 both indicate the highest level of correlation observed between any two residues; negative correlations indicate residue movements correlated in opposing directions.

changes observed in the presence or absence of glutamine. It is important to note that the correlations shown in Figures 6 and 7 are relevant on a nanosecond time scale whereas the steady-state kinetic experiments reported in Figure 5 were acquired on a time scale of seconds to minutes. Consequently, the biochemical and computational results do not necessarily contradict each other. In fact, together these results offer a two-pronged explanation for why T149 and K89 are rigorously conserved in AdT.

Correlations between the residues at the two mutation sites and every other residue for all AdT models provide further insight into the physical connection between GatA and GatB (Figure 8). The T149V mutation shows a significant change in correlation between residues in GatB and position 149 with respect to wild-type AdT; differences between the T149V and wild-type enzymes are much less significant in GatA and GatC (Figure 8A,B). These differences in correlation are enhanced when glutamine is bound to GatA during the simulations. In contrast, a noticeable change in correlation is observed in all three subunits for the K89R mutant compared to the wild-type (Figure 8C,D). This change is also enhanced in the presence of glutamine in GatA. These global variations throughout K89R AdT are consistent with its structural location at the interface between GatA and GatB. Biochemical assays of the K89R mutation show that it has the lowest rate of phosphorylation of all mutations examined in this work (2.8-fold decrease compared to that of wild-type AdT). Combined, these results suggest that K89 plays a vital role in the apparent connectivity between the two active sites.

Root-mean-square deviations (RMSD) for each system were calculated with respect to the crystal structure using the last 10 ns in each simulation. The RMSD calculations were conducted on three different levels: (a) the entire heterotrimeric protein, (2) the individual subunits (GatA, GatB, and GatC), and (3) individual active site residues in GatA [residues 80, 131, 154−156, 174, 176−179, 207, 310, 311, 359, and 426 (termed AS1)] and GatB [residues 6, 10, 12, 79, 91, 124, and 150 (termed AS2)] (see Figure S5 of the Supporting Information). (Note that residues are numbered according to the wild-type AdT sequence from *S. aureus*, not as recorded in the crystal structure PDB file.) The RMSD of GatB showed considerable fluctuation over time, mainly because of movement of the tRNA-binding subdomain (GatB residues 275−412). This subdomain has been proposed to serve as a clamp for Glu-tRNA^{Gln}/Asp-tRNA^{Asn} binding.[26] The high mobility is probably caused by the absence of tRNA in the initial crystal structure as deletion of the contributions of this domain in the RMSD calculation results in a significant reduction in the calculated RMSD of GatB (Figure S5 of the Supporting Information).

dx.doi.org/10.1021/bi201143x | *Biochemistry* 2012, 51, 273−285

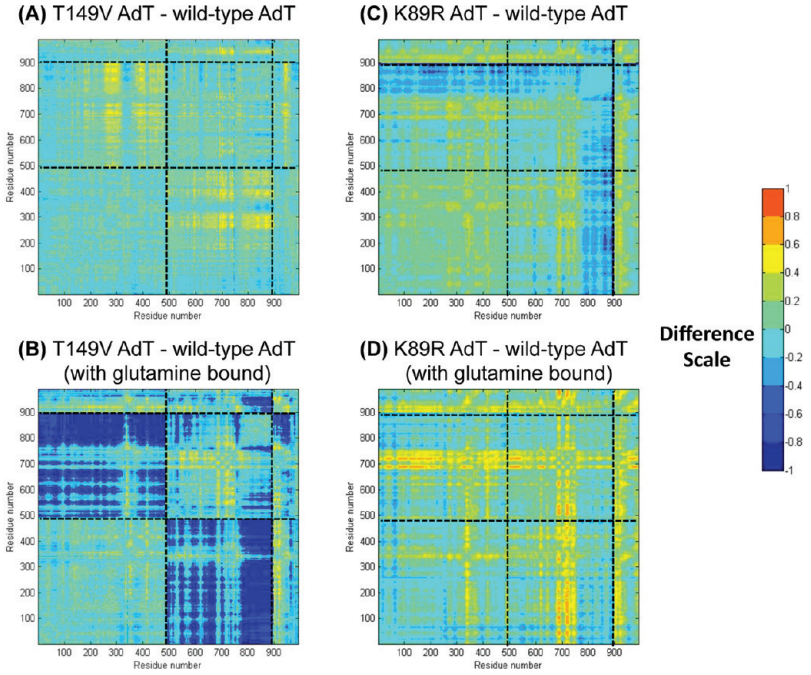

Figure 7. Differences in correlation for each mutant compared to the corresponding wild-type simulation results (wild-type values were subtracted from those of each mutant). (A) Differences between wild-type and T149V AdT. (B) Differences between wild-type and T149V AdT, both in the presence of glutamine. (C) Differences between wild-type and K89R AdT. (D) Differences between wild-type and K89R, both in the presence of glutamine. All panels apply the same color-coded scale representing the calculated correlation differences. See Figure 6 for a key to the different panel subsections.

Average RMSDs ($RMSD_{ave}$) were calculated for each residue in each system over the last 10 ns of each simulation. The differences in $RMSD_{ave}$ between each residue in the mutant versus the wild-type simulations were determined to identify residues that exhibited greater movement in either of the mutant enzymes compared to wild-type AdT. In other words, $\Delta RMSD_{ave}$ = mutant $RMSD_{ave}$ − WT $RMSD_{ave}$. These RMSDs were mapped onto the corresponding simulated structures of AdT (Figure 9).

Percentage RMSD changes were calculated for every residue in both mutant simulations with respect to the corresponding wild-type residue by dividing $\Delta RMSD_{ave}$ by WT $RMSD_{ave}$. This analysis showed that ∼300 residues (<30% of the entire structure) present an $RMSD_{ave}$ change of ≥20%. The residues that showed the highest percentage change from each mutant structure were selected using a 20% change in $RMSD_{ave}$ as an approximate cutoff value for significant change. Of these 300 residues, a subset of 59 residues that is common to both mutant structures was identified. These residues were mapped onto the structure of AdT (Figure 10). These amino acids are distributed throughout all three subunits of AdT and across the full enzyme structure.

The identification of this small subset of residues common to both mutants suggests that they comprise all or part of a pathway for communication between GatA and GatB. For this hypothesis to be correct, these 59 residues should show common patterns of correlation not only between the two mutant enzymes but also in simulations of wild-type AdT. Consequently, correlation analyses[45] were performed for these 59 residues, with and without glutamine in the active site (Figure 11). As expected, these residues are also highly correlated between GatA and GatB in wild-type AdT (Figure 11A,B). Correlation difference plots were also constructed comparing each of these residues from each mutant enzyme to wild-type AdT (Figure 12). These data show that the correlation results demonstrated in Figure 11 do not vary widely between the two mutant enzymes and wild-type AdT. This observation directly supports the hypothesis that these residues are involved in domain−domain communication in AdT, connecting GatA to GatB.

DISCUSSION

Previous enzymological studies of *H. pylori* AdT have predominately focused on its glutaminase and transamidase activities.[25,46] Results from these studies suggest the enhancement of glutaminase activity arises from binding of ATP and Glu-$tRNA^{Gln}$ to the opposing active site. In other words, substrate binding events in the GatB active site are communicated to and impact the efficiency of the GatA active site. This observation suggests the existence of essential connectivities between the GatA and GatB active sites that are sensitive to steps in AdT's reaction pathway. The fact that AdT uses a molecular tunnel to connect its two active sites suggests that this tunnel would be a likely component of AdT's communication network. In this study, mutagenic analyses were used to evaluate conserved residues within the AdT ammonia tunnel, and molecular dynamics simulations were used to further evaluate interdomain communication in this system.

Glu-$tRNA^{Gln}$ was used as the sole aminoacyl-tRNA (aa-tRNA) substrate for AdT (instead of both Glu-$tRNA^{Gln}$ and Asp-$tRNA^{Asn}$). As reported previously, the identity elements for enzyme recognition of the two aa-tRNAs are similar; in particular, they share a common U1:A72 base pair as a key identity element in their acceptor stems.[26,47] To simplify analysis, we chose to focus our efforts on Glu-$tRNA^{Gln}$ as a representative example of the two aa-tRNA substrates for AdT. The adapted enzyme-coupled assay afforded a streamlined way to examine wild-type AdT and its mutants. This approach

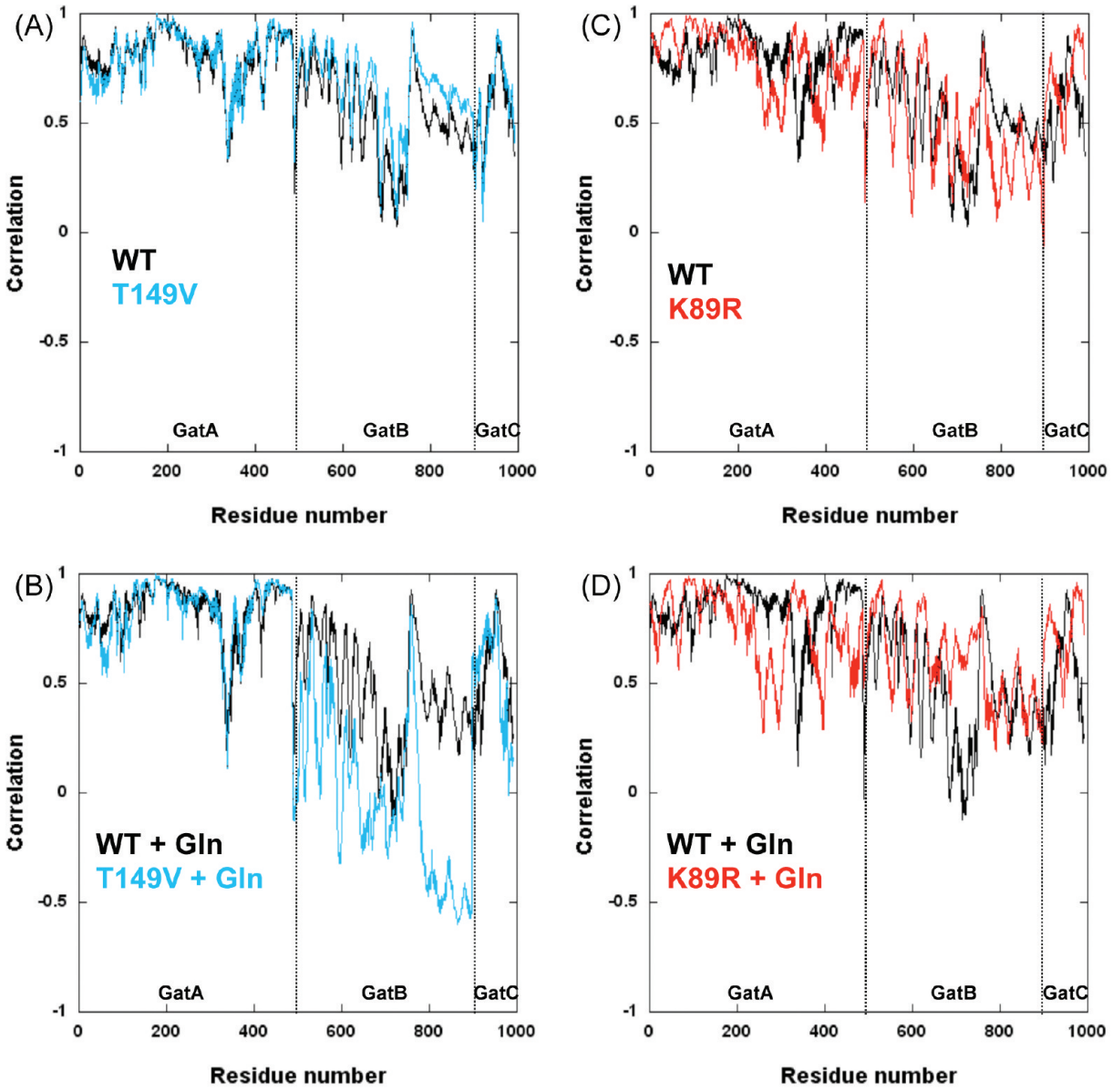

Figure 8. Correlations between each enzyme residue and the T149 and K89 positions (wild-type and mutant AdTs). (A) Comparison between T149 (black) and T149V (cyan) correlations. (B) Comparison between T149 (black) and T149V (cyan) correlations when simulated in the presence of glutamine bound to GatA. (C) Comparison between K89 (black) and K89R (red) correlations. (D) Comparison between K89 (black) and K89R (red) correlations in the presence of glutamine bound to GatA.

provided informative data that allowed us to select the T149V and K89R mutations for molecular dynamics simulations.

Our assay results show that AdT's kinase activity is sensitive to mutations in the GatA glutaminase active site (T149V and T149A) and at the interface between GatA and GatB (R295A, K89A, and Y91F). Mutations near the ATP binding site had little to no effect on activity. Remarkably, the kinase activity of GatB was slightly more susceptible to mutations in GatA, on average, than those in GatB. These observations suggest two things. First, it is unlikely that the observed reductions in kinase activity are due to structural alterations in either active site. In this case, one would expect that GatB mutations would have a greater impact than GatA mutations. Second, these mutations appear to have unmasked communication between GatA and GatB, even though the phosphorylation of misacylated Glu-tRNA^{Gln} is not particularly sensitive to the presence or absence of glutamine in the GatA active site. Previous work on *H. pylori* AdT's glutaminase activity showed that the binding of ATP and Glu-tRNA^{Gln} to GatB enhances the distal glutaminase activity in GatA by ~30-fold.[25] When combined, these analyses have important ramifications for cellular pH homeostasis. They suggest that AdT has evolved to keep its glutaminase activity in check until an aminoacyl-tRNA substrate is available; at this point, glutamine is hydrolyzed to produce ammonia, which is efficiently transferred to the enzyme-bound substrate, rather than released to the intracellular environment.

According to our molecular dynamics simulations, the T149V and K89R AdT mutants showed changes in correlation between GatA and GatB residues compared to those of the wild-type (Figure 6). The presence of glutamine bound to GatA increases the frequency of these changes. The highest level of correlation occurs between GatA and GatB residues in the T149V mutant enzyme with glutamine bound to GatA (Figure 7). Similar patterns of correlation are present for T149V and

dx.doi.org/10.1021/bi201143x | *Biochemistry* 2012, 51, 273−285

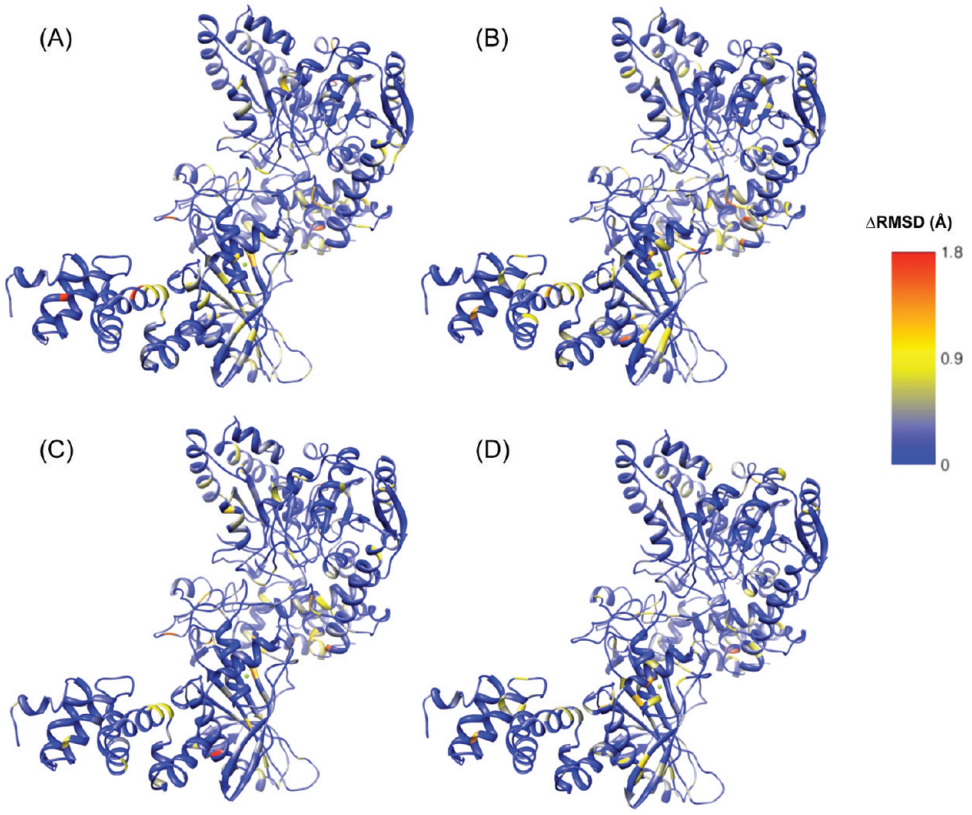

Figure 9. Differences in RMSD (ΔRMSD) for each mutant vs wild-type AdT [wild-type values were subtracted from mutant values (see the text for details)]. (A) ΔRMSD between the T149V AdT simulation, with glutamine bound to GatA, and the AdT structure. (B) ΔRMSD between the T149V AdT simulation in the absence of bound glutamine and the AdT structure. (C) ΔRMSD between the K89R AdT simulation, with glutamine bound to GatA, and the AdT structure. (D) ΔRMSD between the K89R AdT simulation and the AdT structure, in the absence of bound glutamine. The color scheme for panels A–D in angstroms is shown at the right. Larger representations of these figures are provided in Figure S6 of the Supporting Information.

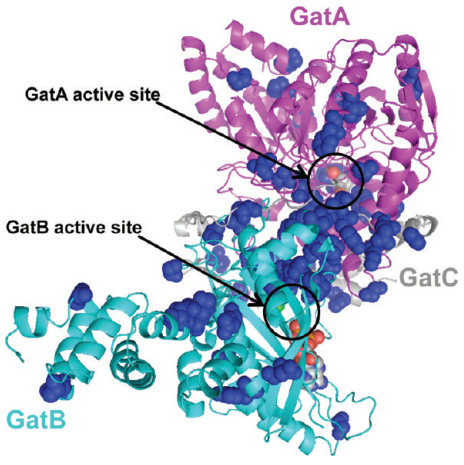

Figure 10. K89R and T149V AdT mutations induce substantial RMSD variations in a common set of 59 residues (RMSD of ≥20% in both mutant enzymes). These residues were mapped onto the *S. aureus Mu50* AdT crystal structure and are highlighted as blue spheres. GatA, GatB, and GatC are colored as in Figure 1 (magenta, cyan, and gray, respectively). The 59 residues are listed in Table S4 of the Supporting Information.

K89R AdT in the absence of glutamine, albeit at significantly lower levels. For wild-type and K89R AdT, this observation is consistent with our kinase assay results that show only slight changes in activity upon the addition of 5 mM glutamine. Conversely, the T149V mutant shows a much higher level of correlation between these motifs in the presence of glutamine, in contrast to the minor reduction observed in kinase activity upon addition of glutamine. It appears that the T149V mutation has reached its maximal impact on kinase activity in the absence of glutamine. However, the simulation results in the presence of glutamine emphasize the extended significance of this mutation with respect to AdT structure and mobility. T149 is immediately adjacent to the glutamine-binding pocket of GatA. Our results suggest that the isosteric conversion of the T149 hydroxyl group to the valine methyl group in the T149V mutation is enough not only to perturb distal kinase activity but also to have a dramatic effect on glutamine binding and communication between the two active sites. Efforts to characterize this enzyme's glutaminase activity are underway.

The correlation patterns of K89 (wild-type) and K89R AdT with all other residues in the enzyme reveal a significant correlation change in all three subunits (Figure 8). When combined, the experimental results show that the K89A and K89R mutations both significantly reduce the initial rate of phosphorylation of Glu-tRNA^{Gln} suggesting that K89 is also involved in interdomain communication.

In addition, significant changes in correlation were observed for both T149V and K89R in areas that connect GatA and GatB (Figure 7), which further supports the hypothesis that a communication pathway exists between these two subunits and that K89 and T149 are influential members of this pathway. The fact that a mutation in GatB (K89R) and a mutation in

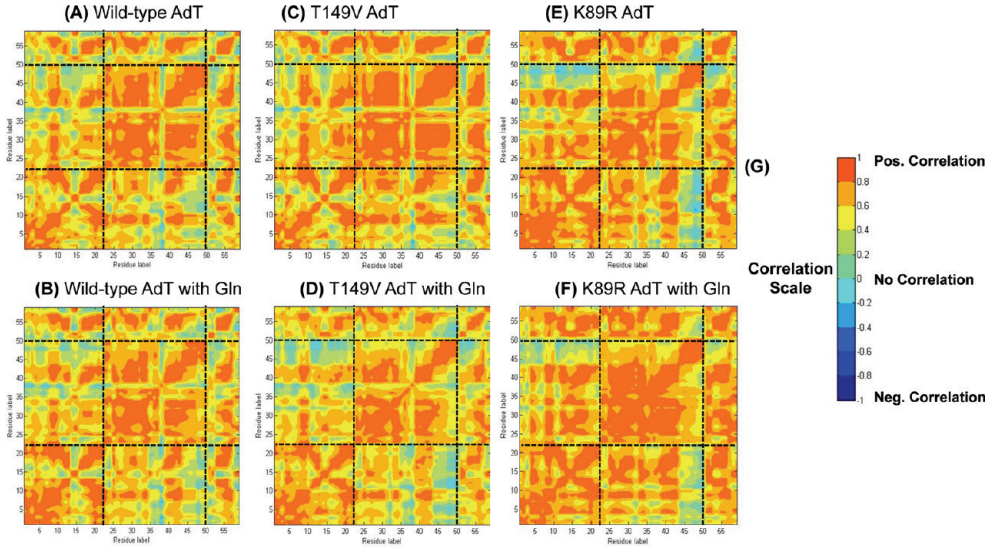

Figure 11. Residue-by-residue correlation of wild-type, T149V, and K89R AdT for the 59 common residues shown in Figure 10. The subsection divisions are the same as in Figure 6. Note that these residues are dispersed throughout the primary sequence of AdT; they are not consecutive. See Table S4 of the Supporting Information for the identity of each residue: (A) wild-type AdT, (B) wild-type AdT with glutamine bound to GatA, (C) T149V AdT, (D) T149V AdT with glutamine bound, (E) K89R AdT, and (F) K89R AdT with glutamine bound. (G) Correlation color scale. As in Figure 6, correlation coefficients of 1 and −1 both indicate the highest level of correlation observed between any two residues; negative correlations indicate residue movements that are correlated in opposing directions.

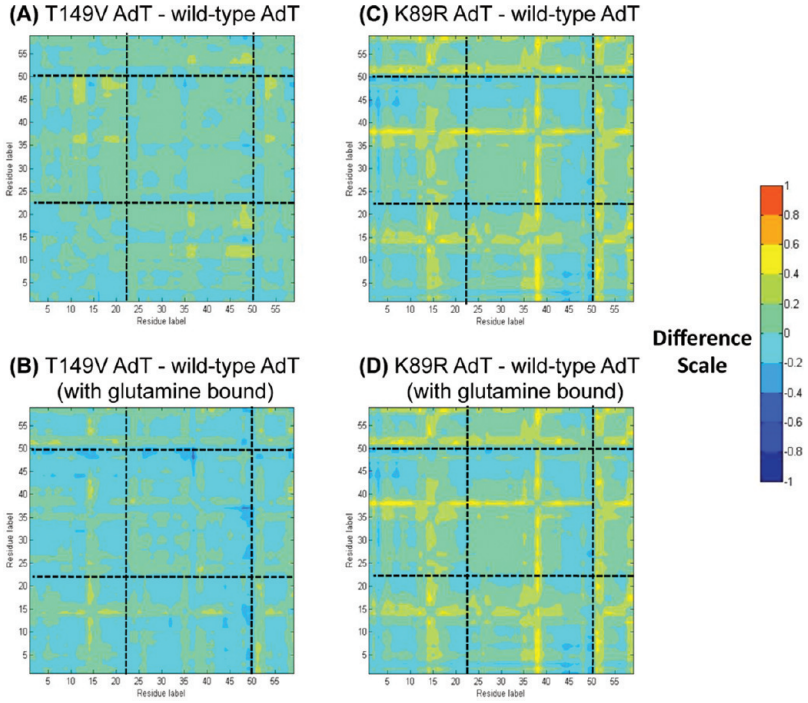

Figure 12. Correlation differences of the 59 common residues for wild-type and K89R AdT. The subsection divisions are the same as in Figure 6. The difference color scale is shown at the right. Note that these residues are dispersed throughout the primary sequence of AdT; they are not consecutive. See Table S4 of the Supporting Information for the identity of each residue: (A) wild-type AdT, (B) wild-type AdT with glutamine bound to GatA, (C) T149V AdT, (D) T149V AdT with glutamine bound, (E) K89R AdT, and (F) K89R AdT with glutamine bound.

GatA (T149V) separately and independently change the correlation pattern between GatA and GatB suggests bidirectionality in communication between GatA and GatB.

The RMSD comparison analysis identified 59 common residues that showed appreciable deviations in both mutant enzymes compared to the wild-type. The fact that these 59 residues are common to both mutant enzymes strongly suggests their involvement in the communication pathway between GatA and GatB. The locations of these 59 residues (see Figure 10) show that they are located in and around the GatA and GatB active sites as well as throughout the region connecting the two sites. A few of the residues are in GatC as well, hinting at a possible role for GatC in mediating communication between GatA and GatB.

Importantly, further analyses of these 59 residues revealed a common correlation pattern connecting GatA to GatB not only

dx.doi.org/10.1021/bi201143x | *Biochemistry* 2012, 51, 273−285

in both mutant enzymes but also in wild-type AdT (Figure 11). This commonality is highlighted by the fact that only moderate differences in correlation were observed upon comparison of each mutant directly to the wild-type (Figure 12). Consequently, these results demonstrate that our MD simulations have unmasked these residues as all or part of an interactive, dynamic, connective path for domain−domain communication in wild-type AdT. Given that K89 and T149 are members of this network and are essential for wild-type AdT activity, it seems probable that these 59 residues offer the first clear evidence of an extensive network of essential interactions throughout AdT.

In conclusion, structural studies work well for the observation of substantial motion in enzyme domains. For example, allosteric rearrangements, loop movements, and domain rotations are often readily visualized by comparing cocrystal structures obtained in the presence of different substrates or ligands. Subtle structural changes can also be examined by crystallography but are sometimes more difficult to assess because of the challenges faced in tying observed residue movement to function. Molecular dynamics simulations are particularly useful for looking at domain−domain communication on a short time scale (nanoseconds). In this work, computational methods allowed us to readily visualize and compare movements in multiple simulations and to assess the impact of functionally interesting mutations. In this way, we were able to identify mobile elements in AdT that might have been difficult to isolate in a crystal structure. The importance of this work goes beyond simply advancing our understanding of how AdT functionally delivers ammonia from GatA to GatB; these results also have implications for other GATs and even other enzymes with apparent domain−domain communication mechanisms.

■ ASSOCIATED CONTENT

Supporting Information

SDS−PAGE analyses of wild-type AdT and all mutations, the effects of NADH concentration on S/N in the kinase enzyme-coupled assay, assay calibration curve, alignment of *S. aureus Mu50* and *H. pylori* AdT primary sequences, RMSD variation with time, and close-ups of Figure 9 (Figures S1−S6) and primers used for site-directed mutagenesis, observed initial rates for wild-type AdT and all mutations in the absence and presence of bound glutamine, and the identities of the 59 common residues analyzed in Figures 11 and 12 (Tables S1−S4). This material is available free of charge via the Internet at http://pubs.acs.org.

■ AUTHOR INFORMATION

Corresponding Author

*Department of Chemistry, Wayne State University, 5101 Cass Ave., Detroit, MI 48202. T.L.H.: telephone, (313) 577-6914; fax, (313) 577-8822; e-mail, tamara.hendrickson@chem.wayne.edu. G.A.C.: telephone, (313) 577-2571; fax, (313) 577-8822; e-mail, andres@chem.wayne.edu.

Present Addresses

[†]Brehm Center, Room 5123, 1000 Wall St., Ann Arbor, MI 48105-1912.

[‡]Department of Chemistry, Wake Forest University, Salem Hall, Winston-Salem, NC 27109.

Funding

This work was financially supported by National Institutes of Health Grant GM071480 to T.L.H. and by Wayne State University funds to G.A.C. and T.L.H.

■ ACKNOWLEDGMENTS

We thank Anastayisa Bordyukova for help in the construction of the pKM049 and pKM050 plasmids, Drs. Stéphane Skouloubris and Pitak Chuawong for plasmids pSS003 and pPTC032, and Wayne State C&IT for computing time.

■ ABBREVIATIONS

AdT, Asp-tRNA^{Asn}/Glu-tRNA^{Gln} amidotransferase; AsnRS, asparaginyl-tRNA synthetase; GAT, glutamine-dependent amidotransferase; GlnRS, glutaminyl-tRNA synthetase; His_6, six-histidine tag; IPTG, isopropyl β-D-1-thiogalactopyranoside; LDH, L-lactate dehydrogenase; MD, molecular dynamics; NAD^+, nicotinamide adenine dinucleotide (oxidized); NADH, nicotinamide adenine dinucleotide (reduced); ND-AspRS, nondiscriminating AspRS; PDB, Protein Data Bank; PEP, phosphoenolpyruvate; PK, pyruvate kinase; RMSD, root-mean-square deviation.

■ REFERENCES

(1) Hyde, C. C., Ahmed, S. A., Padlan, E. A., Miles, E. W., and Davies, D. R. (1988) Three-dimensional structure of the tryptophan synthase $\alpha_2\beta_2$ multienzyme complex from *Salmonella typhimurium*. *J. Biol. Chem. 263*, 17857−17871.

(2) Weeks, A., Lund, L., and Raushel, F. M. (2006) Tunneling of intermediates in enzyme-catalyzed reactions. *Curr. Opin. Chem. Biol. 10*, 465−472.

(3) Raushel, F. M., Thoden, J. B., and Holden, H. M. (2003) Enzymes with molecular tunnels. *Acc. Chem. Res. 36*, 539−548.

(4) Huang, X., Holden, H. M., and Raushel, F. M. (2001) Channeling of substrates and intermediates in enzyme-catalyzed reactions. *Annu. Rev. Biochem. 70*, 149−180.

(5) Miles, E. W., Rhee, S., and Davies, D. R. (1999) The molecular basis of substrate channeling. *J. Biol. Chem. 274*, 12193−12196.

(6) Fitzpatrick, T. B., Amrhein, N., Kappes, B., Macheroux, P., Tews, I., and Raschle, T. (2007) Two independent routes of de novo vitamin B6 biosynthesis: Not that different after all. *Biochem. J. 407*, 1−13.

(7) Williams, L., Fresquet, V., Santander, P. J., and Raushel, F. M. (2007) The multiple amidation reactions catalyzed by Cobyric acid synthetase from *Salmonella typhimurium* are sequential and dissociative. *J. Am. Chem. Soc. 129*, 294−295.

(8) Wojcik, M., Seidle, H. F., Bieganowski, P., and Brenner, C. (2006) Glutamine-dependent NAD^+ synthetase. How a two-domain, three-substrate enzyme avoids waste. *J. Biol. Chem. 281*, 33395−33402.

(9) Ibba, M., Becker, H. D., Stathopoulos, C., Tumbula, D. L., and Soll, D. (2000) The adaptor hypothesis revisited. *Trends Biochem. Sci. 25*, 311−316.

(10) Klem, T. J., and Davisson, V. J. (1993) Imidazole glycerol phosphate synthase: The glutamine amidotransferase in histidine biosynthesis. *Biochemistry 32*, 5177−5186.

(11) Richards, N. G., and Kilberg, M. S. (2006) Asparagine synthetase chemotherapy. *Annu. Rev. Biochem. 75*, 629−654.

(12) Teplyakov, A., Leriche, C., Obmolova, G., Badet, B., and Badet-Denisot, M. A. (2002) From Lobry de Bruyn to enzyme-catalyzed ammonia channelling: Molecular studies of D-glucosamine-6P synthase. *Nat. Prod. Rep. 19*, 60−69.

(13) Kappock, T. J., Ealick, S. E., and Stubbe, J. (2000) Modular evolution of the purine biosynthetic pathway. *Curr. Opin. Chem. Biol. 4*, 567−572.

(14) Evans, D. R., and Guy, H. I. (2004) Mammalian pyrimidine biosynthesis: Fresh insights into an ancient pathway. *J. Biol. Chem. 279*, 33035−33038.

(15) Binda, C., Bossi, R. T., Wakatsuki, S., Arzt, S., Coda, A., Curti, B., Vanoni, M. A., and Mattevi, A. (2000) Cross-talk and ammonia channeling between active centers in the unexpected domain arrangement of glutamate synthase. *Structure 8*, 1299−1308.
(16) Chaudhuri, B. N., Lange, S. C., Myers, R. S., Chittur, S. V., Davisson, V. J., and Smith, J. L. (2001) Crystal structure of imidazole glycerol phosphate synthase: A tunnel through a $(\beta/\alpha)_8$ barrel joins two active sites. *Structure 9*, 987−997.
(17) Larsen, T. M., Boehlein, S. K., Schuster, S. M., Richards, N. G., Thoden, J. B., Holden, H. M., and Rayment, I. (1999) Three-dimensional structure of *Escherichia coli* asparagine synthetase B: A short journey from substrate to product. *Biochemistry 38*, 16146−16157.
(18) Muchmore, C. R., Krahn, J. M., Kim, J. H., Zalkin, H., and Smith, J. L. (1998) Crystal structure of glutamine phosphoribosylpyrophosphate amidotransferase from *Escherichia coli*. *Protein Sci. 7*, 39−51.
(19) Teplyakov, A., Obmolova, G., Badet, B., and Badet-Denisot, M. A. (2001) Channeling of ammonia in glucosamine-6-phosphate synthase. *J. Mol. Biol. 313*, 1093−1102.
(20) Thoden, J. B., Raushel, F. M., Benning, M. M., Rayment, I., and Holden, H. M. (1999) The structure of carbamoyl phosphate synthetase determined to 2.1 Å resolution. *Acta Crystallogr. D55*, 8−24.
(21) Curnow, A. W., Hong, K., Yuan, R., Kim, S., Martins, O., Winkler, W., Henkin, T. M., and Soll, D. (1997) Glu-tRNA^{Gln} amidotransferase: A novel heterotrimeric enzyme required for correct decoding of glutamine codons during translation. *Proc. Natl. Acad. Sci. U.S.A. 94*, 11819−11826.
(22) Ibba, M., and Soll, D. (2000) Aminoacyl-tRNA synthesis. *Annu. Rev. Biochem. 69*, 617−650.
(23) Tomb, J. F., White, O., Kerlavage, A. R., Clayton, R. A., Sutton, G. G., Fleischmann, R. D., Ketchum, K. A., Klenk, H. P., Gill, S., Dougherty, B. A., Nelson, K., Quackenbush, J., Zhou, L., Kirkness, E. F., Peterson, S., Loftus, B., Richardson, D., Dodson, R., Khalak, H. G., Glodek, A., McKenney, K., Fitzegerald, L. M., Lee, N., Adams, M. D., Hickey, E. K., Berg, D. E., Gocayne, J. D., Utterback, T. R., Peterson, J. D., Kelley, J. M., Cotton, M. D., Weidman, J. M., Fujii, C., Bowman, C., Watthey, L., Wallin, E., Hayes, W. S., Borodovsky, M., Karp, P. D., Smith, H. O., Fraser, C. M., and Venter, J. C. (1997) The complete genome sequence of the gastric pathogen *Helicobacter pylori*. *Nature 388*, 539−547.
(24) Cathopoulis, T., Chuawong, P., and Hendrickson, T. L. (2007) Novel tRNA aminoacylation mechanisms. *Mol. BioSyst. 3*, 408−418.
(25) Sheppard, K., Akochy, P. M., Salazar, J. C., and Soll, D. (2007) The *Helicobacter pylori* amidotransferase GatCAB is equally efficient in glutamine-dependent transamidation of Asp-tRNA^{Asn} and Glu-tRNA^{Gln}. *J. Biol. Chem. 282*, 11866−11873.
(26) Nakamura, A., Yao, M., Chimnaronk, S., Sakai, N., and Tanaka, I. (2006) Ammonia channel couples glutaminase with transamidase reactions in GatCAB. *Science 312*, 1954−1958.
(27) Bailly, M., Blaise, M., Lorber, B., Becker, H. D., and Kern, D. (2007) The transamidosome: A dynamic ribonucleoprotein particle dedicated to prokaryotic tRNA-dependent asparagine biosynthesis. *Mol. Cell 28*, 228−239.
(28) Huot, J. L., Balg, C., Jahn, D., Moser, J., Emond, A., Blais, S. P., Chenevert, R., and Lapointe, J. (2007) Mechanism of a GatCAB amidotransferase: Aspartyl-tRNA synthetase increases its affinity for Asp-tRNA(Asn) and novel aminoacyl-tRNA analogues are competitive inhibitors. *Biochemistry 46*, 13190−13198.
(29) Horiuchi, K. Y., Harpel, M. R., Shen, L., Luo, Y., Rogers, K. C., and Copeland, R. A. (2001) Mechanistic studies of reaction coupling in Glu-tRNA^{Gln} amidotransferase. *Biochemistry 40*, 6450−6457.
(30) Kiianitsa, K., Solinger, J. A., and Heyer, W. D. (2002) Rad54 protein exerts diverse modes of ATPase activity on duplex DNA partially and fully covered with Rad51 protein. *J. Biol. Chem. 277*, 46205−46215.
(31) Kowalczykowski, S. C., and Krupp, R. A. (1987) Effects of *Escherichia coli* SSB protein on the single-stranded DNA-dependent ATPase activity of *Escherichia coli* RecA protein. Evidence that SSB protein facilitates the binding of RecA protein to regions of secondary structure within single-stranded DNA. *J. Mol. Biol. 193*, 97−113.
(32) Gasteiger, E., Hoogland, C., Gattiker, A., Duvaud, S., Wilkins, M. R., Appel, R. D., and Bairoch, A. (2005) Protein Identification and Analysis Tools on the ExPASy Server. In *The Proteomics Protocols Handbook* (Walker, J. M., Ed.) pp 571−607, Humana Press, Totowa, NJ.
(33) Skouloubris, S., Ribas de Pouplana, L., De Reuse, H., and Hendrickson, T. L. (2003) A noncognate aminoacyl-tRNA synthetase that may resolve a missing link in protein evolution. *Proc. Natl. Acad. Sci. U.S.A. 100*, 11297−11302.
(34) Chang, K. M., and Hendrickson, T. L. (2009) Recognition of tRNAGln by *Helicobacter pylori* GluRS2: A tRNA^{Gln}-specific glutamyl-tRNA synthetase. *Nucleic Acids Res. 37*, 6942−6949.
(35) Feng, L., Sheppard, K., Tumbula-Hansen, D., and Soll, D. (2005) Gln-tRNA^{Gln} formation from Glu-tRNA^{Gln} requires cooperation of an asparaginase and a Glu-tRNA^{Gln} kinase. *J. Biol. Chem. 280*, 8150−8155.
(36) Case, D. A., Cheatham, T. E. III, Darden, T., Gohlke, H., Luo, R., Merz, K. M. Jr., Onufriev, A., Simmerling, C., Wang, B., and Woods, R. J. (2005) The Amber biomolecular simulation programs. *J. Comput. Chem. 26*, 1668−1688.
(37) Ryckaert, J. P., Ciccotti, G., and Berendsen, H. J. C. (1977) Numerical Integration of Cartesian Equations of Motion of a System with Constraints: Molecular Dynamics of N-Alkanes. *J. Comput. Phys. 23*, 327−341.
(38) Essmann, U., Perera, L., Berkowitz, M. L., Darden, T., Lee, H., and Pedersen, L. G. (1995) A Smooth Particle Mesh Ewald Method. *J. Chem. Phys. 103*, 8577−8593.
(39) York, D. M., Darden, T. A., and Pedersen, L. G. (1993) The Effect of Long-Range Electrostatic Interactions in Simulations of Macromolecular Crystals: A Comparison of the Ewald and Truncated List Methods. *J. Chem. Phys. 99*, 8345−8348.
(40) Chen, V. B., Arendall, W. B. III, Headd, J. J., Keedy, D. A., Immormino, R. M., Kapral, G. J., Murray, L. W., Richardson, J. S., and Richardson, D. C. (2010) MolProbity: All-atom structure validation for macromolecular crystallography. *Acta Crystallogr. D66*, 12−21.
(41) Pettersen, E. F., Goddard, T. D., Huang, C. C., Couch, G. S., Greenblatt, D. M., Meng, E. C., and Ferrin, T. E. (2004) UCSF Chimera: A visualization system for exploratory research and analysis. *J. Comput. Chem. 25*, 1605−1612.
(42) Berendsen, H. J. C., Postma, J. P. M., Vangunsteren, W. F., Dinola, A., and Haak, J. R. (1984) Molecular-Dynamics with Coupling to an External Bath. *J. Chem. Phys. 81*, 3684−3690.
(43) Sheppard, K., Akochy, P. M., Salazar, J. C., and Soll, D. (2007) The *Helicobacter pylori* amidotransferase GatCAB is equally efficient in glutamine-dependent transamidation of Asp-tRNA^{Asn} and Glu-tRNA^{Gln}. *J. Biol. Chem. 282*, 11866−11873.
(44) Wu, J., Bu, W., Sheppard, K., Kitabatake, M., Kwon, S. T., Soll, D., and Smith, J. L. (2009) Insights into tRNA-dependent amidotransferase evolution and catalysis from the structure of the *Aquifex aeolicus* enzyme. *J. Mol. Biol. 391*, 703−716.
(45) Kaledin, M., Kaledin, A. L., Brown, A., and Bowman, J. M. (2006) Driven Molecular Dynamics for Normal Modes of Biomolecules without the Hessian, and Beyond. In *Normal Mode Analysis: Theory and Applications to Biological and Chemical Systems* (Cui, Q., and Bahar, I., Eds.) pp 281−300, Chapman and Hall/CRC, Boca Raton, FL.
(46) Cathopoulis, T. J., Chuawong, P., and Hendrickson, T. L. (2007) A thin-layer electrophoretic assay for Asp-tRNA^{Asn}/Glu-tRNA^{Gln} amidotransferase. *Anal. Biochem. 360*, 151−153.
(47) Bailly, M., Giannouli, S., Blaise, M., Stathopoulos, C., Kern, D., and Becker, H. D. (2006) A single tRNA base pair mediates bacterial tRNA-dependent biosynthesis of asparagine. *Nucleic Acids Res. 34*, 6083−6094.